INTERNATIONAL ATOMIC ENERGY AGENCY
UNITED NATIONS EDUCATIONAL, SCIENTIFIC AND CULTURAL ORGANIZATION
INTERNATIONAL CENTRE FOR THEORETICAL PHYSICS
I.C.T.P., P.O. BOX 586, 34100 TRIESTE, ITALY. CABLE: CENTRATOM TRIESTE

SMR.478 - 21

THIRD AUTUMN COURSE ON MATHEMATICAL ECOLOGY

(29 October - 16 November 1990)

"Finite Element Analysis of Long Period Tidal Propagation in a Channel"

Hock-Lye KOH
Universiti Sains Malaysia
School of Mathematical Sciences
11800 Penang
Malaysia

These are preliminary lecture notes, intended only for distribution to participants.

Finite Element Analysis of Long Period Tidal Propagation in a Channel

H.L. KOH
Universiti Sains Malaysia,Malaysia

INTRODUCTION

Scarcity of land available for further growth in Penang has induced the local authority to reclaim coastal areas around Penang by landfill. Of late, several schemes have been proposed to reclaim various sites for commercial, industrial and residential use. One of these schemes aims to reclaim land on the mainland Butterworth side. Figure 1 indicates the location of the reclamation site, shown shaded, to the eastern mid section of the Southern Channel.

Located 5 km to the north of the reclamation site is the Penang deep water wharf, whose proper functioning should not be adversely affected by the reclamation. Hence, an analysis of the flow regimes in the Southern Channel becomes a prerequisit to the issuing of permit for such a reclamation. In this paper, we present a finite element analysis of tidal propagations through the Southern Channel.

THE STUDY SITE

Located between the Penang Island and Butterworth at Lat 5^{o} 25'N and Long 100^{o} 21'E, Southern Channel is about 22 km long and varies in width from 2 km at the Throat Section (at Georgetown) to 14 km to the south at D. The bottom topography is highly irregular but generally aligned to the north-south axis. Figure 2 shows the depth profiles at two east-west cross sections, namely the Throat Section at the latitude of Georgetown and the Middle Section shown with dashed lines in Figure 1. The east-west cross sectional area varies between 4×10^{4} to 4.5×10^{4} m^2. The currents are driven predominantly by the semi-diurnal tides passing through the channel, with a mean spring tidal amplitude of 1 m and a mean neap tidal amplitude of 0.25 m. Figure 3 shows the cumulative discharges through the Throat Section and the Middle Section for spring

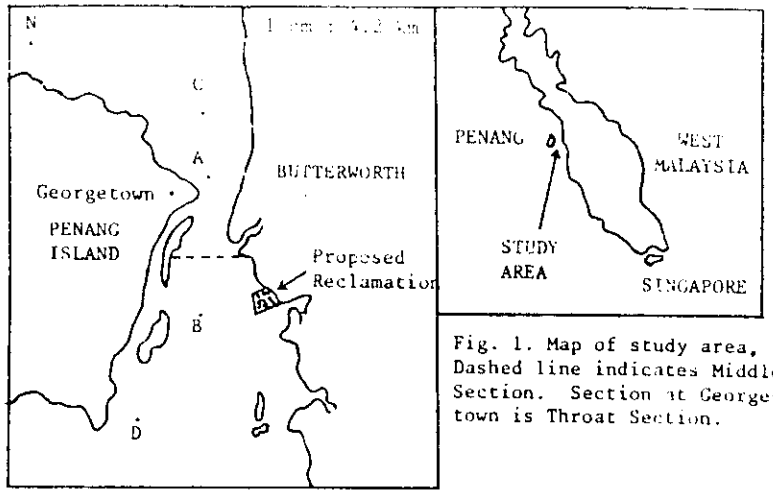

Fig. 1. Map of study area, Dashed line indicates Middle Section. Section at Georgetown is Throat Section.

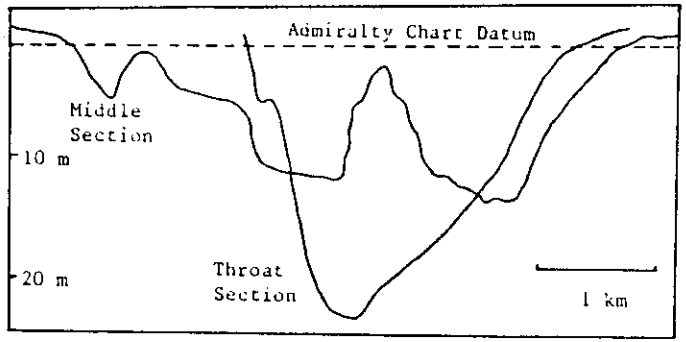

Fig. 2. Depth profiles at two cross sections

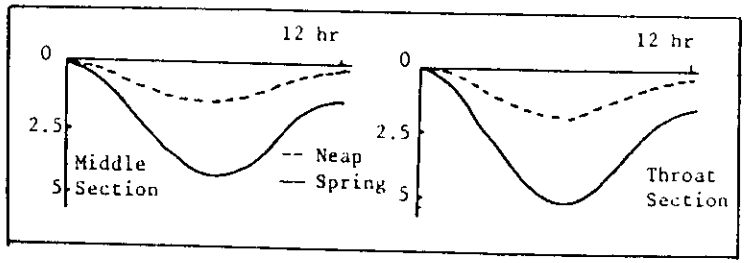

Fig. 3. Cumulative discharges at two cross sections ($10^6 m^3$)

and neap tides. The maximum current speed is about 1 m/s during spring tide and 0.30 m/s during neap tide. The currents flow due south during flood tide and due north during ebb tide. Long term averaged hourly data on current velocities and tidal heights are available for locations marked A and B in Figure 1. These data will be used in the finite element model calibration and validation. Tidal heights at location C are ahead of those at location D by about 52 minutes. The maximum current is ahead of the extreme water by about 30 minutes.

GOVERNING EQUATIONS

Data on temperature and salinity in the Southern Channel indicate that the water column is vertically well-mixed[1]. Hence the following vertically integrated two dimensional shallow water hydrodynamic model is appropriate. Here the pressure is hydrostatic and the two horizontal velocity components in the x (east) and y (north) vertically integrated.

$$\frac{\partial H}{\partial t} + \frac{\partial (Hu)}{\partial x} + \frac{\partial (Hv)}{\partial y} = 0, \tag{1}$$

$$\frac{\partial u}{\partial t} + u\frac{\partial u}{\partial x} + v\frac{\partial u}{\partial y} + g\frac{\partial \zeta}{\partial x} - fv + \frac{ku\sqrt{u^2+v^2}}{H} + E_{xx} - \frac{\tau^x}{H} = 0 \tag{2}$$

$$\frac{\partial v}{\partial t} + u\frac{\partial v}{\partial x} + v\frac{\partial v}{\partial y} + g\frac{\partial \zeta}{\partial y} + fu + \frac{kv\sqrt{u^2+v^2}}{H} + E_{yy} - \frac{\tau^y}{H} = 0 \tag{3}$$

where g is gravity, ζ the distance from mean sea level to the water surface, H the total water depth, f the coriolis parameter, and k the dimensionless bottom friction coefficient. Further E_{xx} and E_{yy} are the turbulent eddy viscosity in the x and y directions respectively, and finally τ^x, τ^y are the wind stresses conceived to act as a body force throughout the water column, whose magnitude is given by Wu^2.

The boundary conditions imposed are the specification of zero normal flow to a land boundary and the specification of water elevation at a boundary open to sea, river input being negligible.

GALERKIN FINITE ELEMENT FORMULATION

Various finite element formulations to the shallow water equations are available[3-5]. In this paper quadrilateral isoparametric elements[6] are used as basis functions.

Weighting the residual of equation (2) with N_j to zero, we obtain

$$\iint \left\{ \frac{\partial u}{\partial t} + u\frac{\partial u}{\partial x} + v\frac{\partial u}{\partial y} + g\frac{\partial \zeta}{\partial x} + w \right\} . N_j \, dA = 0. \tag{4}$$

where W represents the remaining terms in (2) for convenience. Other equations are dealt with similarly. These give rise to a set of ordinary differential equations in time.

The time derivatives are replaced by a semi-implicit finite difference scheme that involves 3 time levels per iteration. The terms to be treated implicitly are the divergence terms in the mass conservation equation and the pressure gradient, eddy viscosity and wind stress terms in the momentum equations. All other terms are treated explicitly. Denoting terms treated explicitly by E and those implicitly by I, we may express the differential equations (4) symbolically by

$$\frac{dg}{dt} = E + I. \tag{5}$$

In these notations, the semi-implicit scheme becomes

$$\frac{g(t + \Delta t) - g(t - \Delta t)}{2\Delta t} = E(t) + \{I(t + \Delta t) + I(t - \Delta t)\} \tag{6}$$

This yields a linear system of algebraic equations with time-invariant coefficient matrix that can be inverted once and for all and where time marching is not severely restricted by the Courant stability criteria for a fully explicit scheme.

STABILITY AND CONVERGENCE

This semi-implicit scheme is stable with time steps $\Delta t = 3$ minutes, which is some 20 times larger than those allowed by the Courant criteria. However with Δt much larger than 3 minutes, local instability begins to show up, particularly at the Throat Section. The constriction at the Throat Section appears to be the cause of this local instability, judging from numerical tests on wedge shaped channels of similar dimension but with flat bottom. The highly irregular bottom topograph (Figure 2) also appears to cause local instability as is observed by model numerical tests with straight channels of same dimension but with irregular bottom. Hence it is necessary to carefully smooth out the bottom topography, in such a manner that cross sectional area is preserved in each element, noting that the flow direction is generally along the north-south axis. Local instability is also observed near the sea boundary which could be controlled by the use of slightly higher eddy viscosity for elements adjacent to the sea boundary.

When the model is initiated with zero water elevation and zero current velocities, it takes generally 4 to 5 tidal cycles to achieve dynamic steady state periodic solution. However, with a good guess of initial conditions obtained by simple adjustments from previous results, dynamic convergence can be attained in 1 to 2 tidal cycles, hence saving computation time.

RESULTS AND DISCUSSION

Boundary conditions imposed on the sea boundary are the sine functions $\alpha \sin(\omega t + \eta)$, where α is the tidal amplitude, ω corresponds to the semi-diurnal tide and η the phase lag, whose values are assigned 0 at D and 0.44 at C corresponding to a phase lag of 52 minutes between C and D. Values of α are assigned to equal 1 m for spring tide, 0.25 m for neap tide, and 0.50 m for an average tide.

Current data at locations A and B for a mean spring tide are used to calibrate the model. The calibration value for the dimensionless bottom friction coefficient k is finally adjusted at 0.0025 with slightly higher value near the land boundary. The computed results are validated by data at locations A and B for a mean neap tide. Figures 4 shows the comparisons between computed and measured current speeds at locations A and B for spring and neap tide, which appear to be reasonably good. We define the residual flow over a tidal cycle of period T by

$$\frac{1}{T}\int_0^T v(t)dt.$$

Figure 5 shows the residual flow during a spring tidal cycle (under condition of no wind), which varies from a low of 0.3 cm/s in the southern end of the channel to a high of 5.1 cm/s around the Throat Section and is due south. During a neap tidal cycle, the residual flow is much smaller.

To test the effect of wind on the residual flow, a wind of 4.5 m/s due south in effect for a complete tidal cycle is used. This wind, by itself, generates a residual flow that varies from 1.3 cm/s to 2.3 cm/s during a spring tide and from 2.8 cm/s to 5.2 cm/s during a neap tide. Wind in the reverse direction generates similar effects.

Figure 3 depicts the cumulative discharges through the Throat and Middle Sections for a spring and a neap tide. During a spring tidal cycle, there is a net transport due south of magnitude 125 million m^3 while the corresponding figure during a neap tide is a 12 million m^3 also due south. With a wind of 4.5 m/s due south in effect for a tidal cycle, the corresponding net transports due south are 160 million m^3 and 89 million m^3 respectively. This means that this wind generates a net transport per tidal cycle of 35 million m^3 and 77 million m^3 respectively. It should be noted that the dorminant wind direction is due south and south-west which occurs for 35 % of the time.

Finally Figure 6 and 7 show the velocity plots at two instances, namely during flood and ebb tide respectively, for a spring tide.

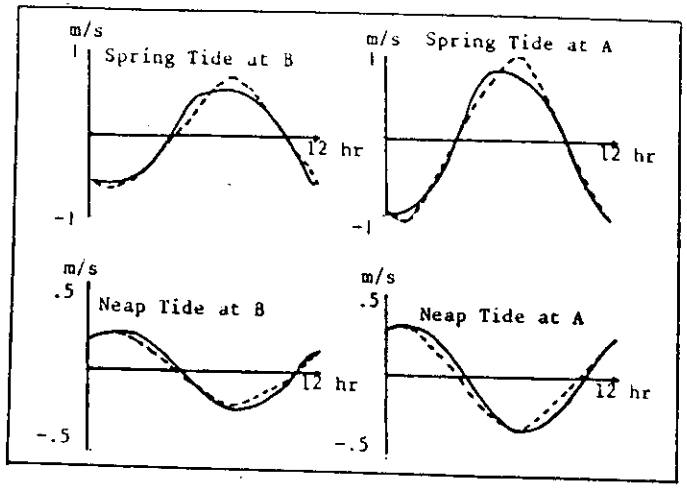

Fig. 4. Computed (-) verses measured (---) velocity

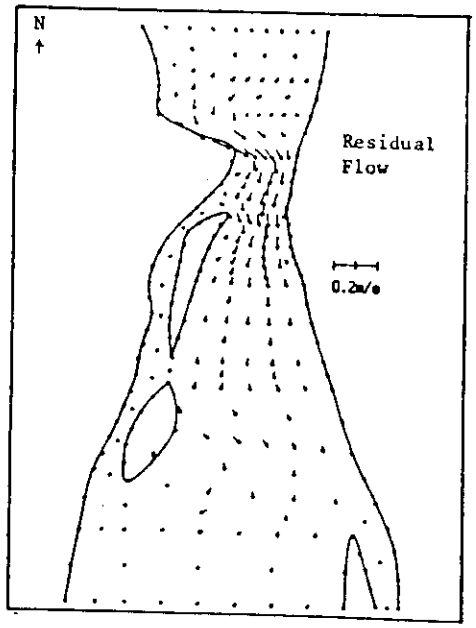

Fig. 5. Residual flow for spring tide

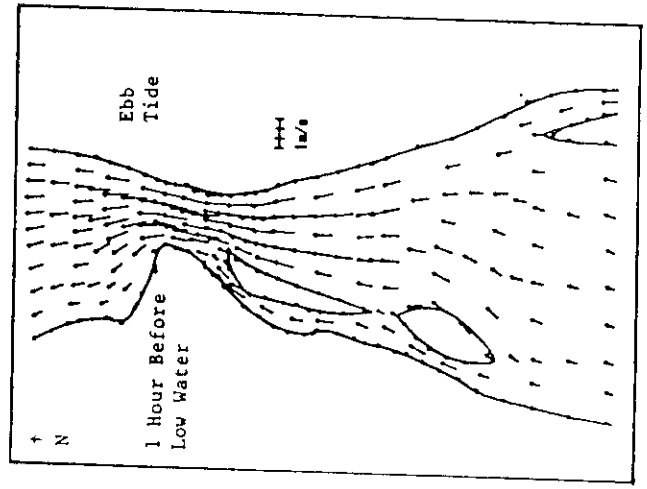

Fig. 7 Velocity plot for spring tide.

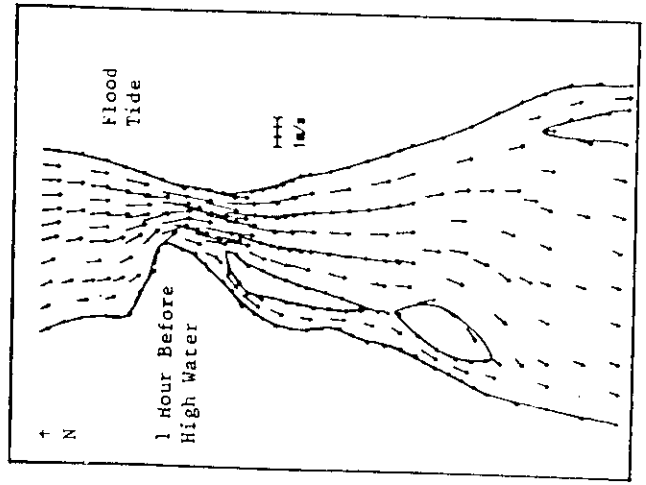

Fig.6. Velocity plot for spring tide

The results presented here are useful to decision makers concerned with the reclamation project.

ACKNOWLEDGEMENT

A generous financial grant from the Penang Development Corporation who commissioned this study is gratefully acknowledged.

REFERENCES

1. H.L. Koh and D. Zubir: "Coastal Oceanographic Study of the Straits of Penang", A Consultancy Report to the Penang Development Corporation, Malaysia, 1987.

2. J. Wu: "Wind Stress and Surface Roughness at Air-Sea Interface", Journal Geophysics Res, Vol 74, No. 2, 1969, pp 444 - 455.

3. J. Goussebaile, F. Hecht, G. Labadie, and L. Reinhart: "Finite Element Solution of the Shallow Water Equations by a Quasi-Direct Decomposition Procedure", Int. Journal for Numerical Methods in Fluid, Vol 4, 1984, pp 1117 - 1136.

4. M. Kawahara, S. Nakazawa, S. Ohmori and T. Tagaki: "Two-Step Explicit Finite Element Method for Storm Surge Proposition Analysis", Int. Journal for Numerical Methods in Engineering, Vol 15, 1980, pp 1129 - 1148.

5. M. Kawahara, M. Kobayashi and K. Nakata: "Multiple Level Finite Element Analysis and its applications to Tidal Current Flow in Tokyo Bay", Appl. Math. Modelling, Vol 7, 1983, pp 197 - 211.

6. R.A. Walters and R.T. Cheng: "A Two-Dimensional Hydrodynamic Model for A Tidal Estuary", Proceddings of Second International Conference on Finite Elements in Water Resources (Ed: C.A. Brebbia, W.G. Gray and G.F. Pinder), Pentech Press, London, 1978, pp 2.3 - 2.21.